Geophysical Research Letters

Supporting Information for

Ultra-low surface temperatures in East Antarctica from satellite thermal infrared mapping: the coldest places on Earth

T. A. Scambos[1], G. G. Campbell[1], A. Pope[1], T. Haran[1], A. Muto[2]

M. Lazzara[3], C. H. Reijmer[4] and M. R. van den Broeke[4]

[1] National Snow and Ice Data Center, University of Colorado at Boulder, Boulder CO 80303 USA. [2] Department of Earth and Environmental Science, Temple University, Philadelphia, PA 19122 USA. [3] Antarctic Meteorological Research Center, University of Wisconsin-Madison and Madison Area Technical College, Madison, WI 53706 USA. [4] Institute for Marine and Atmospheric Research, Utrecht University, Utrecht NL-3584, Netherlands

Contents of this file

Introduction

The table and figures below provide further background on the land surface temperature data examined for the study, and provide supporting evidence of clear-sky conditions for the observed temperatures. The supplemental table describes the determination of the near-surface air temperature gradient at the Dome A AWS, which is referred to in the text and used in estimating the difference between surface snow temperatures from thermal emission data and the extrapolated surface (0 m) air temperature. Additional evidence of the occurrence of ultra-low temperatures in high-elevation shallow topographic depressions is included in profile data extracted from the compiled minimum surface temperatures and surface elevation as provided by a DEM (Bamber et al., 2009). We also show additional examples of the time-series of temperatures at near-record low temperature sites, demonstrating that adjacent grid cells in the compiled image data set show very similar temperatures during the events (i.e. demonstrating that the sites are not spurious data points) and that the time-series data show very slow cooling rates below -90°C followed by abrupt warming. The relationship between the Southern Annular Mode strength (as indicated by the Marshall, 2003 index) and the frequency and extent of very cold surface temperatures is provided here, and referred to in the main text. Finally, two figures illustrate the processes controlling the observed minimum temperature (downwelling radiation from clear, extremely dry atmosphere) and the overall conceptual model for the ultra-low temperature event occurrences.

Table S1. Winter cold-event Air Temperature Gradients at Dome A AWS, 2008-2014[a]

	2008	2009	2010	2011	2012	2013	2014
Mean height, '4m' sensor[b]:	3.50	3.62	3.50	3.46	3.41	3.25	3.15
Number of AWS hourly reports:	681	327	888	228	929	414	525
Mean cold-event temperature, °C -							
'4m':	-69.1	-66.8	-70.1	-67.5	-66.8	-65.4	-64.2
'2m':	-73.0	-71.3	-73.3	-71.3	-71.1	-71.2	-69.6
'1m':	-75.6	-74.9	-75.5	-73.9	-75.6	-76.9	-75.6
Estimated surface temperature, °C -							
	-76.5	-76.5	-76.2	-74.6	-76.1	-77.0	-75.2
Mean air temp. gradient °C m^{-1}:	2.1	2.7	1.8	2.1	2.8	3.7	3.6

Weighted mean surface temperature from linear trend of air temperatures during low-temperature events: -76.1±0.4°C
Weighted mean air temperature gradient during low-temperature events: 2.7°C m^{-1}

[a]Cold events extracted from hourly AWS data, 15 June – 15 September, defined by LST c6 surface temperatures <-73°C
[b]Elevation of '4m' air temperature sensor assuming 4.0 m height above surface on installation in January 2005; adjusted using Dome A AWS snow height data

Figure S1. Results of a pilot study of lowest observed surface snow temperatures in AVHRR and MODIS data sets.

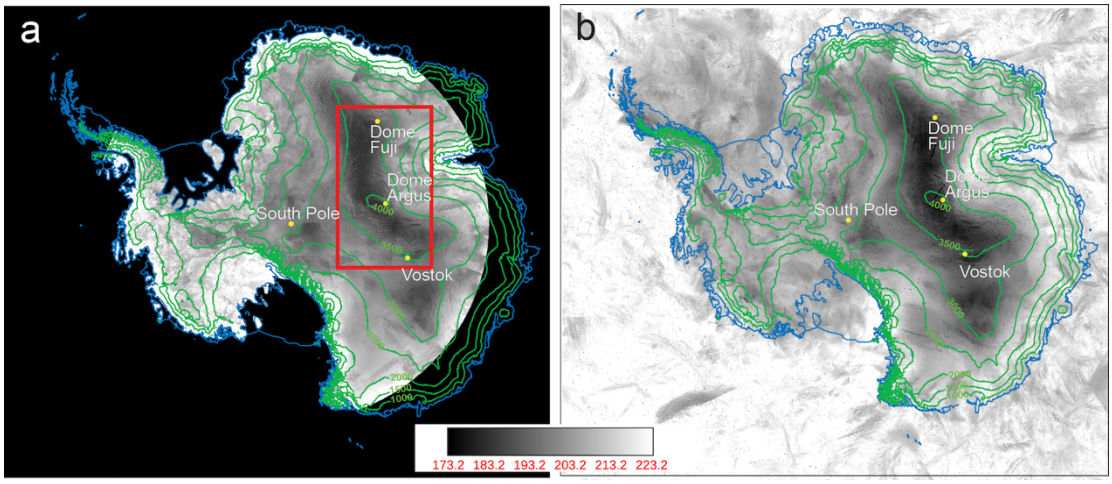

Figure S1. Image maps of the lowest grid cell temperature values for Antarctica from (a) south of 70°S on the Antarctic grounded ice sheet in the MODIS MYD011 Land Surface Temperature data set (Wan, 2006; Wang et al., 2013) for 15 June to 15 September only, during 2004-2016 (1 km grid resolution); and (b) from the AVHRR Polar Pathfinder ice surface temperature from the entire Antarctica polar stereo grid for all dates in the data set spanning 1982-2000 (5 km grid resolution; Key et al., 1997; Wang and Key, 2005), based on thermal emission temperature from band pairs in the 10 – 11µ thermal bands. Temperature range is -100°C to -50°C (scale bar in Kelvins). Elevation contours (at 500 m spacing are shown in green (Bamber et al., 2009), ice sheet coastline and grounding line in blue (Haran et al., 2014). The red box in (a) indicates the main study area shown in Figure 1 of the main text.

Figure S2. Lowest observed temperatures, shaded relief topography, individual MODIS LST image, and visible-band mosaic of the Dome A region, demonstrating the close relationship between observed thermal structure of the lowest observed temperatures and the local topography of the ice sheet.

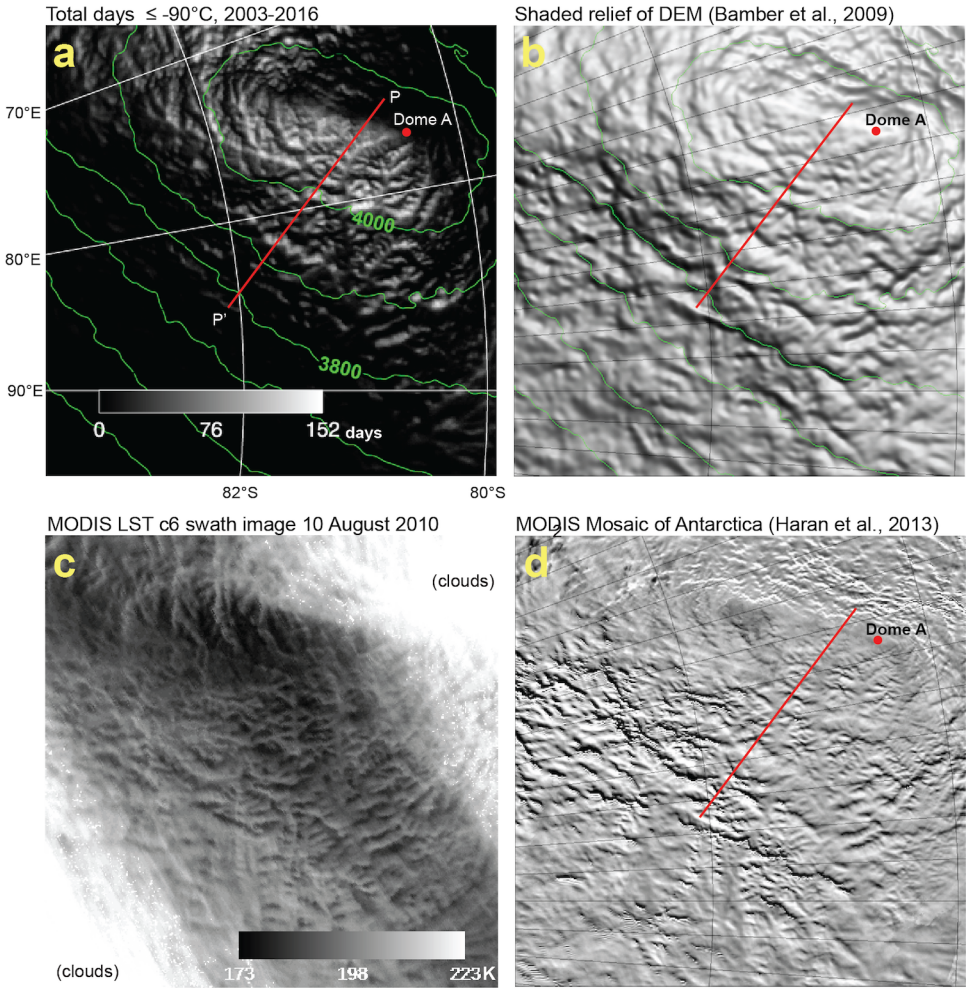

Figure S2. Comparison maps of (a) number of days with occurrences of surface snow temperatures ≤-92°C for 2004-2016 from MODIS LST c6 for the area near Dome A, East Antarctica (80.367°S, 77.350°E); (b) Satellite-data-derived DEM of the same region (Bamber et al., 2009); (c) single swath of MODIS Aqua thermal image acquired on 10 August 2010 showing the detailed visibility of the local topography in a surface temperature image; and (d) MODIS composite image of surface morphology (MOA2009; Haran et al., 2014). Image maps are 400 by 400 km. The similarity in spatial structure indicates that the low temperature periods are not influenced by clouds. Red circle is the Dome A summit, 4093 m a.s.l. Red line P-P' is the extracted 250km profile in Figure S3, combining (a) and (b) data.

Figure S3. Profile of frequency of ultra-low temperatures (<-90°C), lowest observed temperature, and topography of Dome A, for the P-P' profile in Figure S2, showing the close relationship between topographic depressions and low-temperature occurrences.

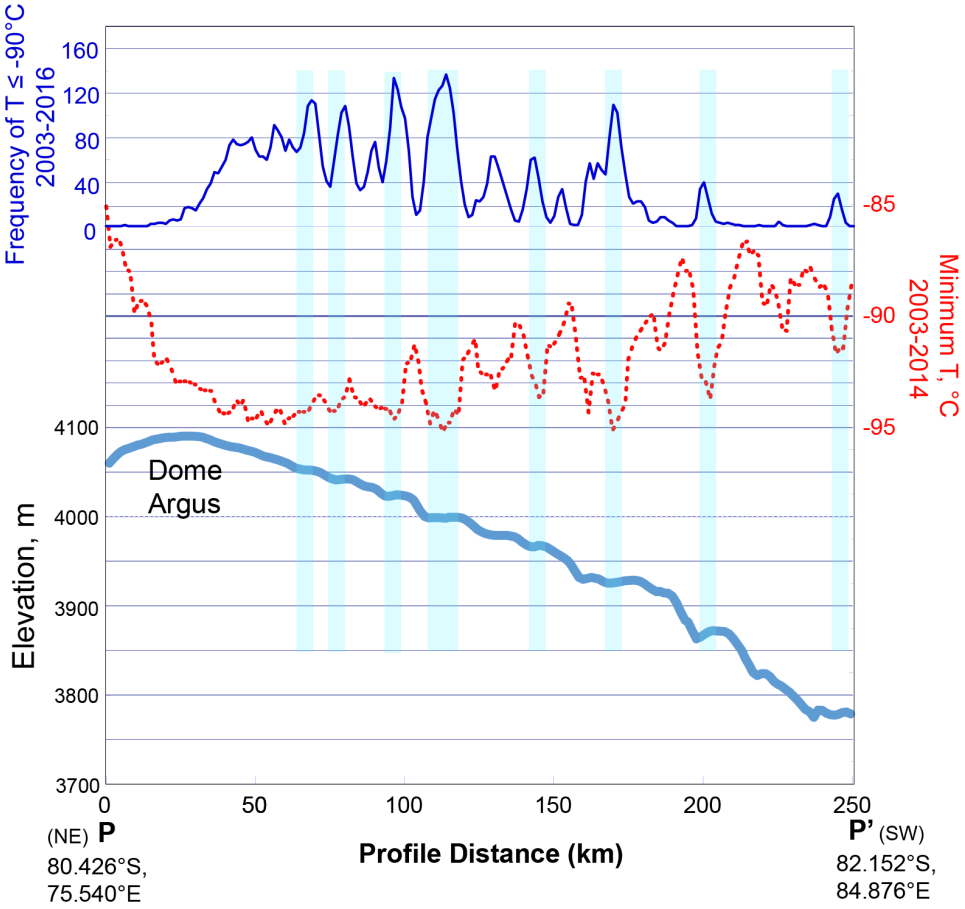

Figure S3. Profiles of elevation, ultra-low surface temperature occurrences, and lowest observed temperatures near Dome A along profile P-P' in Figure S2. Top profile indicates total number of days between day of year 180 (June 29 or 28) and day of year 250 (September 6 or 7) spanning 2003 to 2016 when MYD11 c6 or MOD11 c6 indicated a temperature of -90°C at least once. Middle profile is minimum temperature recorded in the MYD11 c6 data set between the same dates spanning 2003 to 2014. Bottom profile is an elevation transect across Dome A based on Bamber et al., 2009 data (datum is WGS84 ellipsoid). The vertical blue bars indicate the regions where the slope in the transect is < 0.001 or reversed.

Figure S4. Additional plots of time-series of observed MODIS LST c5 and c6 data around ultra-low temperature events. The plots demonstrate that adjacent grid cells show very similar cooling and warming patterns, and that the different data versions corroborate each other, and provide further examples indicating very slow cooling rates as observed temperatures drop below -90°C.

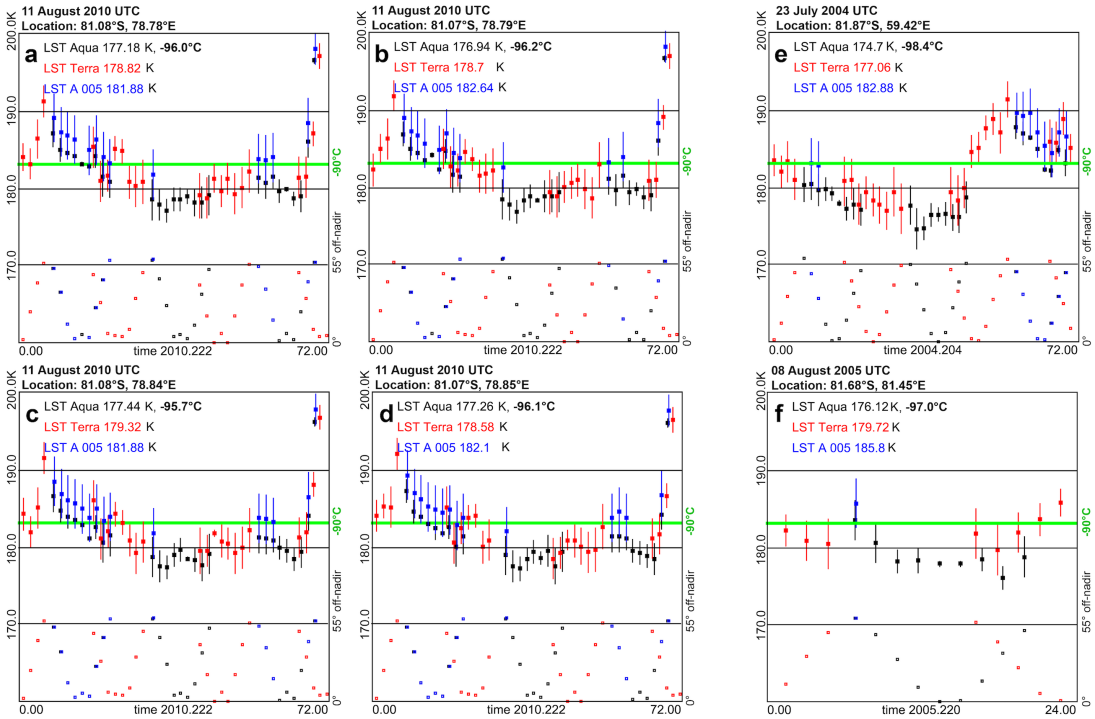

Figure S4. Upper part of the panels show MODIS LST time-series of selected grid cells for surface temperature versus time. Lower section of the panels indicate off-nadir viewing angle for the MODIS LST swaths. Error bars for the LST data are based on viewing parameters and estimated water vapor in the view path. Panels a-d, four adjacent LST grid cells during a single low-temperature event in 2010. Panels e and f, additional examples of time-series data for cold events.

Figure S5. Relationship between frequency of occurrence of low or ultra-low temperatures and the Southern Annular Mode index.

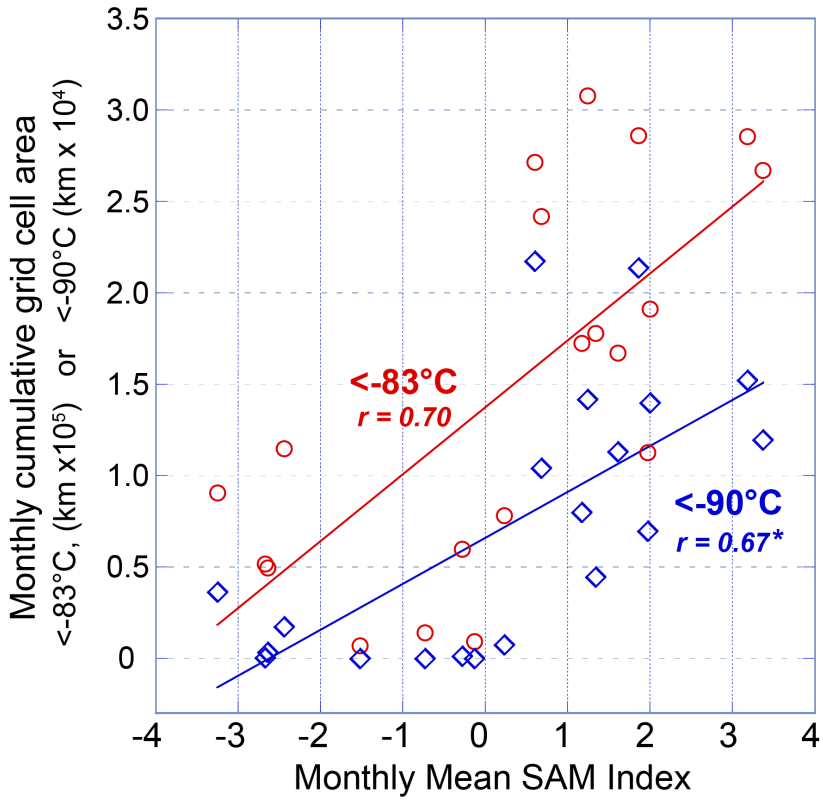

Figure S5. Monthly mean Southern Annular Mode (SAM) index (Marshall, 2003; Marshall et al., 2016) versus total area of grid cells exhibiting surface temperatures below -83°C and -90°C for July and August, 2006 to 2015. Regression value for -90°C is compromised since several months with negative SAM index values have zero area reported.

Figure S6. The emission spectra of high-emissivity (snow) surface at very low terrestrial temperatures shows peak thermal emission within the atmospheric absorption features of CO2 and water vapor. The graph below shows the high sensitivity of water vapor transmissivity in the far infrared region to water vapor column length in the atmosphere. Comparing the upwelling surface emission at, e.g., -95°C and the downwelling clear-air emission at, e.g. 25 atm-cm water vapor shows that thermal emission is very nearly balanced (and therefore cooling rates of the surface would be very low).

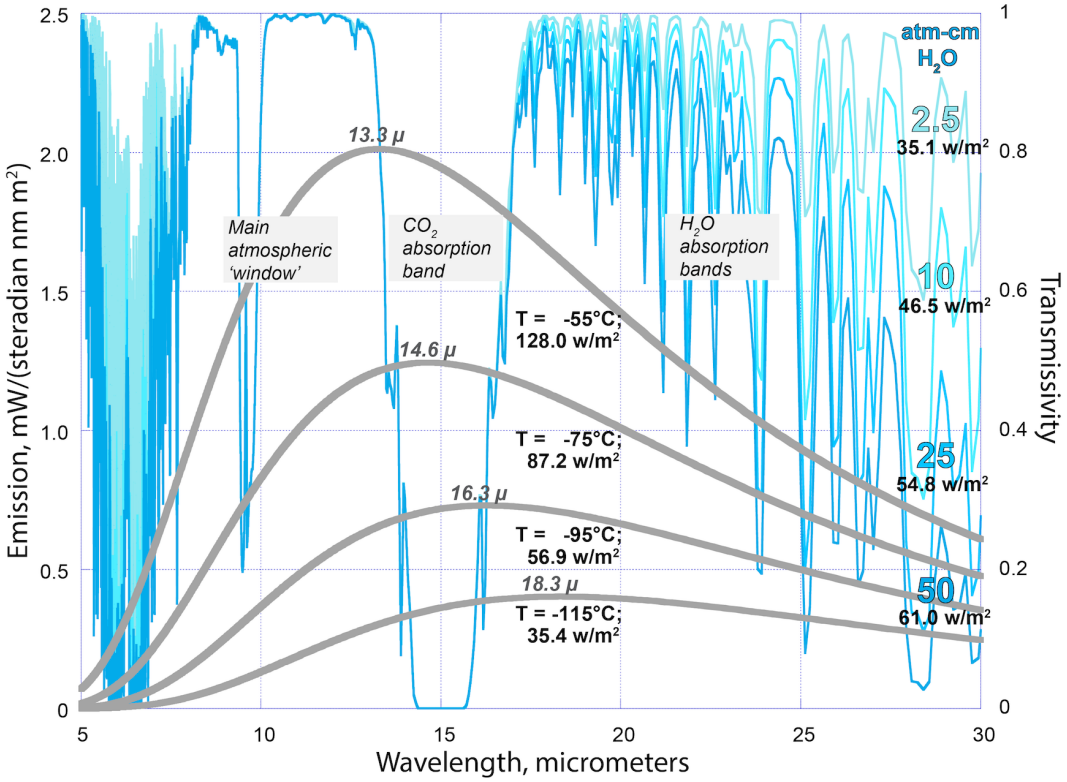

Figure S6. Comparison of upwelling surface thermal radiance from a snow surface at a range of low temperatures and downwelling thermal radiance from an atmosphere with a similar temperature profile to the ultra-cold events and having a range of very low water vapor contents. Thermal radiance of the snow surface was calculated assuming ε = 0.997, similar to dry fine-grained snow. Atmosphere transmissivity was derived from MODTRAN® (Berk et al., 2014; also, University of Chicago website at http://climatemodels.uchicago.edu/modtran) using the "subarctic winter" atmospheric temperature profile offset by -30°C. This produced a similar temperature profile to that of mid-winter South Pole determined by balloon-borne profilers. Viewing was set to 'upward' from 3.8 km altitude. Default values for CO_2, CO, CH_4 and O_3 were used. Transmissivity is shown for four different water vapor levels, with resulting net downwelling radiance for the air column (right side of graph). Water vapor columns,

with units of atm-cm, are roughly equal to precipitable water in the air column times 1000. Peak emission wavelengths of the four emission spectra are shown on the graph, as well as the net upward radiance.

Figure S7. Summary diagram of the processes and physical conditions discussed in the study.

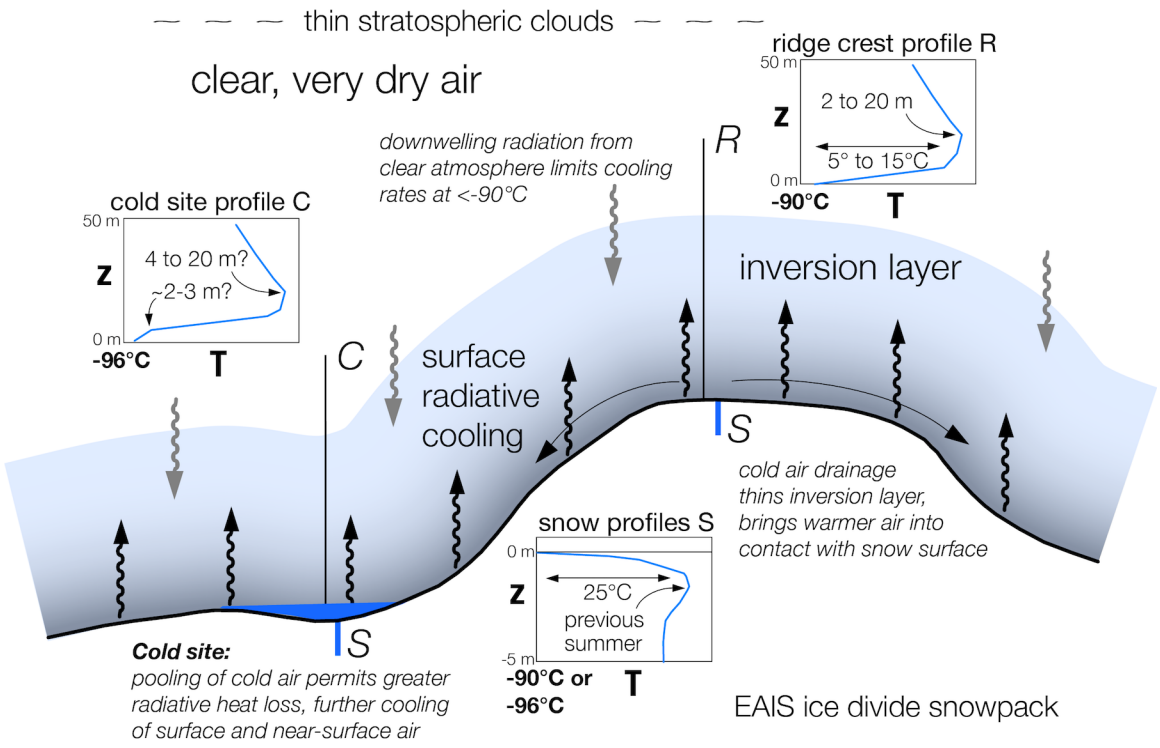

Figure S7. Schematic diagram of processes and near-surface conditions at ultra-low surface temperature sites.